



# Spatial and temporal variability of $p\text{CO}_2$ and $\text{CO}_2$ emissions from the Dong River in south China

Boyi Liu<sup>1</sup>, Mingyang Tian<sup>2</sup>, Kaimin Shih<sup>3</sup>, Chun Ngai Chan<sup>1</sup>, Xiankun Yang<sup>4</sup>, and Lishan Ran<sup>1</sup>

<sup>1</sup>Department of Geography, the University of Hong Kong, Hong Kong SAR, China

<sup>2</sup>Institute for Geology, Center for Earth System Research and Sustainability (CEN), Universität Hamburg, Hamburg, Germany

<sup>3</sup>Department of Civil Engineering, University of Hong Kong, Hong Kong SAR, China

<sup>4</sup>School of Geographical Sciences, Guangzhou University, Guangzhou, 510006, China

**Correspondence:** Lishan Ran (lsran@hku.hk)

Received: 19 December 2020 – Discussion started: 11 January 2021

Revised: 26 August 2021 – Accepted: 27 August 2021 – Published: 27 September 2021

**Abstract.**  $\text{CO}_2$  efflux at the water–air interface is an essential component of the riverine carbon cycle. However, the lack of spatially resolved  $\text{CO}_2$  emission measurements prohibits reliable estimation of the global riverine  $\text{CO}_2$  emissions. By deploying floating chambers, seasonal changes in river water  $\text{CO}_2$  partial pressure ( $p\text{CO}_2$ ) and  $\text{CO}_2$  emissions from the Dong River in south China were investigated. Spatial and temporal patterns of  $p\text{CO}_2$  were mainly affected by terrestrial carbon inputs (i.e., organic and inorganic carbon) and in-stream metabolism, both of which varied due to different land cover, catchment topography, and seasonality of precipitation and temperature. Temperature-normalized gas transfer velocity ( $k_{600}$ ) in small rivers was  $8.29 \pm 11.29$  and  $4.90 \pm 3.82 \text{ m d}^{-1}$  for the wet season and dry season, respectively, which was nearly 70 % higher than that of large rivers ( $3.90 \pm 5.55 \text{ m d}^{-1}$  during the wet season and  $2.25 \pm 1.61 \text{ m d}^{-1}$  during the dry season). A significant correlation was observed between  $k_{600}$  and flow velocity but not wind speed regardless of river size. Most of the surveyed rivers were a net  $\text{CO}_2$  source while exhibiting substantial seasonal variations. The mean  $\text{CO}_2$  flux was  $300.1$  and  $264.2 \text{ mmol m}^{-2} \text{ d}^{-1}$  during the wet season for large and small rivers, respectively, 2-fold larger than that during the dry season. However, no significant difference in  $\text{CO}_2$  flux was observed between small and large rivers. The absence of commonly observed higher  $\text{CO}_2$  fluxes in small rivers could be associated with the depletion effect caused by abundant and consistent precipitation in this subtropical monsoon catchment.

## 1 Introduction

River networks act as a processor that transfers and emits the carbon entering the water, rather than just a passive pipe that transports carbon from the terrestrial ecosystem to the ocean (Cole et al., 2007; Battin et al., 2009; Drake et al., 2018).  $\text{CO}_2$  emissions at the water–air interface are an essential component of the riverine carbon cycle.  $\text{CO}_2$  emitted from inland waters to the atmosphere reaches up to  $2.9 \text{ Pg C yr}^{-1}$ , surpassing that transported from land to ocean through rivers (Sawakuchi et al., 2017; Drake et al., 2018). Understanding the role that rivers play in the global carbon cycle is still hindered by uncertainty on the flux estimate of  $\text{CO}_2$  emissions from rivers (Cole et al., 2007; Raymond et al., 2013; Sawakuchi et al., 2017; Drake et al., 2018). Riverine carbon emissions have significant temporal and spatial variations, making it challenging to accurately quantify carbon emissions. In addition, watershed geomorphology, hydrological conditions, climate, and other environmental factors can affect the  $\text{CO}_2$  efflux in rivers (Alin et al., 2011; Abril et al., 2014; Almeida et al., 2017; Ran et al., 2017a; Borges et al., 2018). Thus, there are substantial differences in  $\text{CO}_2$  efflux among rivers in different climate regions or the same river but between different seasons (Denfeld et al., 2013; Rasera et al., 2013). An enhanced understanding of the temporal and spatial characteristics of the water–air  $\text{CO}_2$  flux will facilitate a more robust estimate. However, global riverine  $\text{CO}_2$  emission estimates were largely based on data disproportionately focusing on temperate and boreal regions, including North

America and Europe (Raymond et al., 2013; Lauerwald et al., 2015; Drake et al., 2018). More studies are required in other data-poor regions to achieve a more accurate estimate.

Rivers in tropical and subtropical regions of East Asia and Southeast Asia are among those underrepresented regions that need more attention since they are essential participants in riverine carbon transport (Ran et al., 2015, 2017b; Drake et al., 2018). The high temperature in this region facilitates a high net primary productivity in the terrestrial ecosystem and intense biochemical activities; both contribute to the carbon input dynamic from soil to rivers (Li et al., 2018). Meanwhile, rivers in this region are under the heavy influence of monsoon climate, and riverine  $\text{CO}_2$  emissions vary significantly among seasons due to the changes in temperature and precipitation. In addition, different rivers in this region may have contrasting trends in  $\text{CO}_2$  dynamic due to different underlying controlling factors. Some rivers have the highest  $\text{CO}_2$  efflux in the wet season (Li et al., 2013; Le et al., 2018; Ni et al., 2019), while others have the highest  $\text{CO}_2$  efflux in the dry season (Luo et al., 2019), suggesting that an increase in the wet season runoff can have two distinct consequences. On the one hand, recent studies have indicated that the increased runoff could enhance external carbon inputs and thus  $\text{CO}_2$  emissions (Hope et al., 2004; Johnson et al., 2008). On the other hand, the increased runoff may result in a dilution of the dissolved  $\text{CO}_2$  in rivers and accordingly a reduction in  $\text{CO}_2$  emissions (Ran et al., 2017b; Li et al., 2018). Therefore, it is important to investigate the underlying processes that determine the diverse responses of  $\text{CO}_2$  emissions to the monsoon climate.

The Dong River (DJR), located in subtropical south China, is one of the three tributaries of the Pearl River. Previous studies on riverine carbon transport and emissions in the Pearl River system mainly focused on the Xi River, which is characterized by widely distributed carbonate rocks, and the estuary area of the Pearl River delta (Yao et al., 2007; Zhang et al., 2015, 2019, 2021). Although some studies on chemical weathering and dissolved inorganic carbon (DIC) transport in the Dong River basin (DJRB) have been conducted (Tao et al., 2011; Fu et al., 2014), there is still a lack of understanding of the characteristics of catchment-wide  $\text{CO}_2$  emissions from the DJRB. Furthermore, a predominantly hilly landscape combined with abundant precipitation favors the formation of a great number of small rivers in the DJRB (Ding et al., 2015). However, current estimates of basin-wide  $\text{CO}_2$  emissions from the river network are mostly based on the data from large rivers, and small rivers are heavily underrepresented (Raymond et al., 2013; Drake et al., 2018). Because the controlling factors and the input of carbon could be significantly different between large and small rivers (Johnson et al., 2008; Dinsmore et al., 2013; Hotchkiss et al., 2015; Marx et al., 2017), a more comprehensive quantification of  $\text{CO}_2$  emissions from small headwater streams is necessary. Therefore, studies on the characteristics of riverine  $\text{CO}_2$  emissions from the DJRB should be conducted among

river size spectrums, and the impact of monsoon needs to be considered.

By using directly measured river water  $\text{CO}_2$  partial pressure ( $p\text{CO}_2$ ) and  $\text{CO}_2$  emission data from the DJRB and in conjunction with hydrological and physicochemical data, the objectives of this study were to (1) investigate the spatial and temporal pattern of  $p\text{CO}_2$  and  $\text{CO}_2$  emissions along stream size spectrum and (2) examine the differences in hydrological and physicochemical controls on  $p\text{CO}_2$  and  $\text{CO}_2$  emissions between small headwater streams and large rivers. The results of this study will shed light on the underlying controls of the spatial and temporal distribution of riverine  $p\text{CO}_2$  and support a refined estimate of regional and global carbon budgets.

## 2 Material and methods

### 2.1 Site description

The DJR in south China is one of the three major tributaries of the Pearl River system (Fig. 1). It has a 562 km long mainstem channel and a drainage area of 35 340 km<sup>2</sup> (Chen et al., 2011). Due to its subtropical monsoon climate, precipitation in the DJRB exhibits significant seasonal variability (Fig. 2a). The multi-annual average precipitation is about 1800 mm, 80 % of which is concentrated during the wet season from April to September. The Boluo Hydrological Gauge is the lowermost gauge of the Dong River mainstem channel, controlling a drainage area of  $\sim 23\,000$  km<sup>2</sup>. The multi-annual average water discharge at Boluo Hydrological Gauge is 23.7 km<sup>3</sup> (Zhang et al., 2008). About 80 %–90 % of the discharge is transported during the wet season (Fig. 2b). The landscape is characterized by plains and hills, accounting for 87.3 % of the river basin area (Ding et al., 2015), and the dominant land use of the catchment is highly diverse evergreen forests of broadleaved and needleleaf species (Ran et al., 2012; Chen et al., 2013). The impacts of human activities on land use vary among three regions in the DJRB. Urban expansion and agricultural activities have substantially altered the land use in the lower and middle Dong River basin (LDJRB and MDJRB), respectively, while the upper Dong River basin (UDJRB) is less affected by human activities (Fig. 1).

### 2.2 Field measurements and analyses

In total, there were 43 sampling sites spanning seven Strahler stream orders. Fourth- to seventh-order streams were mainstem and major tributaries, while first- to third-order streams were small tributaries. River widths were measured by a laser rangefinder. Sampled rivers were categorized, according to their stream orders, into small rivers (first- to third-order streams, SR) and large rivers (fourth- to seventh-order streams, LR). The small rivers had an average width of  $15.4 \pm 10.2$  m, while large rivers have an average width of  $180.3 \pm 159.3$  m (Table S1). Those sampling sites were

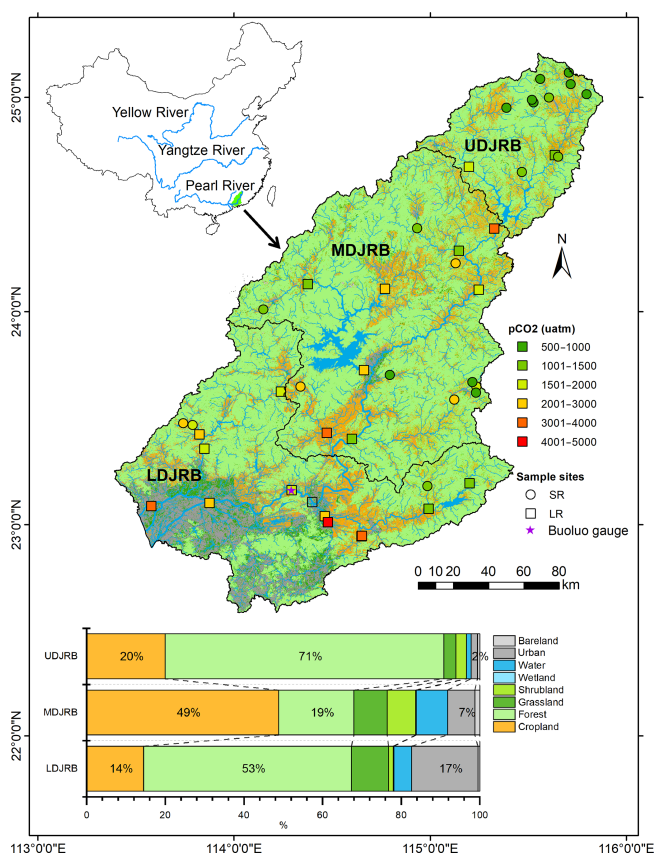


**Figure 1.** Sample sites and land cover in the DJRB. Yearly average  $p\text{CO}_2$  at each sample site was displayed. Based on the land cover dataset FROM-GLC10 (<http://data.ess.tsinghua.edu.cn>, last access: 17 September 2021).

widely distributed in the mainstem and nine major sub-catchments among the three regions with different topographic features and land cover (Fig. 1). In order to investigate  $\text{CO}_2$  emissions during different hydrological conditions, we performed five fieldwork campaigns from December 2018 to October 2019, including three in the wet season (early wet season – late April, middle wet season – early July, and late wet season – late August) and two in the dry season (middle dry season – December 2018 to early January 2019 and early dry season – late October 2019). Sample sites were measured in the daytime over 2 weeks for each field trip. Three campaigns in the wet season allowed each sample site to be measured under different hydrological conditions. As for the dry season, the hydrological condition was relatively stable due to low precipitation. However, field measurements conducted during the daytime could lead to an underestimate in  $p\text{CO}_2$  and  $\text{CO}_2$  emissions (Reiman and Xu, 2019a). Nocturnal  $\text{CO}_2$  emission rates in rivers could be 27 % greater than the daytime rates (Gómez-Gener et al., 2021). During the field trips, water temperature, pH, and dissolved oxygen (DO) were measured with a portable multi-parameter probe (Multi 3430, WTW GmbH, Germany). The

pH probe was calibrated before each field trip with standard pH buffers (4.01 and 7.00). Measurements were conducted 10 cm below the water surface. To evaluate the contribution of metabolism on DO changes,  $\Delta\text{CO}_2$  and  $\Delta\text{O}_2$  were calculated as described by Stets et al. (2017) using

$$\Delta\text{CO}_2 = \text{CO}_{2w} - \text{CO}_{2a} \quad (1)$$

and

$$\Delta\text{O}_2 = \text{O}_{2w} - \text{O}_{2a}, \quad (2)$$

where  $\text{CO}_{2w}$  and  $\text{O}_{2w}$  are measured concentrations of  $\text{CO}_2$  and  $\text{O}_2$  in a water sample, while  $\text{CO}_{2a}$  and  $\text{O}_{2a}$  are the equilibrium  $\text{CO}_2$  and  $\text{O}_2$  concentrations ( $\mu\text{mol L}^{-1}$ ).

Flow velocity was determined by using a global water flow probe FP111 with a precision of  $0.1 \text{ m s}^{-1}$ , while wind speed at 1.5 m above the water surface was measured with a Kestrel 2500 handheld anemometer and normalized to a height of 10 m ( $U_{10}$ ) using the equation from Alin et al. (2011). As the flow velocity was measured near the riverbanks, an underestimation of the flow velocity is possible. Flow velocity measured near the riverbanks is only about 40 % of the maximum flow velocity at the cross section (Moramarco et al., 2004; Le Coz et al., 2008). We also collected water for analyzing total alkalinity (TA) and dissolved organic carbon (DOC). Firstly, 100 mL of water samples was filtered through a pre-combusted glass fiber filter (pore size:  $0.47 \mu\text{m}$ , Whatman GF/F, GE Healthcare Life Sciences, USA). Then, 50 mL of water used for TA analysis was titrated with  $0.1 \text{ mol L}^{-1}$  HCl on the same day of sampling. The remaining 50 mL of water for DOC analysis was poisoned with concentrated  $\text{H}_2\text{SO}_4$  to  $\text{pH} < 2$  and preserved in a cooler with ice bags before analysis. DOC was determined by the high-temperature combustion method using a TOC analyzer (Elementar Analysensysteme GmbH, Langensfeld, Germany) that has a precision better than 3 %.

### 2.3 Calculation of $p\text{CO}_2$ and $\text{CO}_2$ emission flux

The surface water  $p\text{CO}_2$  was determined using the headspace equilibrium method, which could avoid the possible overestimation of using TA and pH to calculate  $p\text{CO}_2$  in rivers with a relatively low pH (Abril et al., 2015). We used a 625 mL reagent bottle to collect 400 mL of water from  $\sim 10$  cm below the surface, leaving 225 mL of space filled with ambient air as headspace. The bottle was then immediately capped and shaken vigorously for at least 1 min to achieve an equilibrium between the water and the  $\text{CO}_2$  in the headspace (Hope et al., 1994). Then, the bottle was connected to the calibrated Li-850  $\text{CO}_2 / \text{H}_2\text{O}$  gas analyzer (Li-Cor, Inc, USA), and the equilibrated gas in this closed loop was measured. The measurements at each site were repeated twice, and the average was then calculated. The variation between the two measurements was less than 5 %, and the accuracy of Li-850 is within 1.5 % of the reading. The ambient air  $p\text{CO}_2$  ( $p\text{CO}_2^{\text{air}}$ )

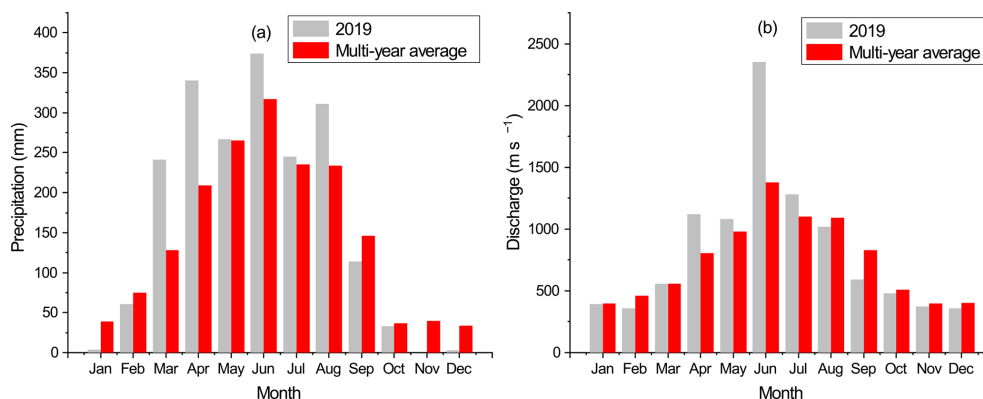


**Figure 2.** Monthly variations in (a) precipitation of the DJRB and (b) water discharge at the Boluo hydrological gauge, based on data provided by the Hydrological Bureau of Guangdong Province.

was measured before the headspace measurements and the chamber deployments. The  $p\text{CO}_2^{\text{air}}$  value varied between 380 and 450  $\mu\text{atm}$ . The original surface water  $p\text{CO}_2$  ( $p\text{CO}_2^{\text{water},i}$ ) was finally calculated by using solubility constants ( $K_0$ ) for  $\text{CO}_2$  from Weiss (1974), carbonate constants ( $K_1$ ,  $K_2$ ) from (Millero et al., 2006), and the volume of the flask, headspace, and residual system (line and gas analyzer) (Dickson et al., 2007; Ran et al., 2017a; Tian et al., 2019) using

$$p\text{CO}_2^{\text{water},i} = p\text{CO}_2^{\text{headspace},f} + \left( \frac{V_h + V_r}{V_w} \right) \left( p\text{CO}_2^{\text{h+r}} - p\text{CO}_2^{\text{headspace},i} \right) / \left[ RTK_0 \left( 1 + \frac{K_1}{[\text{H}^+]} + \frac{K_1K_2}{[\text{H}^+]^2} \right) \right], \quad (3)$$

where  $V_h$ ,  $V_r$ , and  $V_w$ , are the headspace volume, residence system volume, and water volume, respectively.  $R$  is the universal gas constant ( $8.314 \text{ J mol}^{-1} \text{ K}^{-1}$ ),  $T$  is the water temperature in kelvin (K), and  $[\text{H}^+]$  is the concentration of hydrogen ions.  $p\text{CO}_2^{\text{headspace},i}$  and  $p\text{CO}_2^{\text{headspace},f}$  are  $p\text{CO}_2$  before and after the headspace equilibration, respectively.  $p\text{CO}_2^{\text{h+r}}$  is the  $p\text{CO}_2$  of the mixed gas in the headspace and residual system during the measurement. The  $p\text{CO}_2^{\text{headspace},i}$  was taken as the  $p\text{CO}_2$  in ambient air before the measurement, while  $p\text{CO}_2^{\text{headspace},f}$  was calculated using

$$p\text{CO}_2^{\text{headspace},f} = p\text{CO}_2^{\text{h+r}} + \left( \frac{V_r}{V_h} \right) \left( p\text{CO}_2^{\text{h+r}} - p\text{CO}_2^{\text{headspace},i} \right). \quad (4)$$

To measure  $V_r$ , we filled the headspace with ambient air, which had a known  $p\text{CO}_2$ , and measured the  $p\text{CO}_2$  in the closed loop.  $V_r$  was then estimated according to Eq. (3). A comparative analysis of the syringe and bottle headspace method has been conducted to evaluate the accuracy of the headspace extraction method used in this study (Table S2 and

Fig. S2). Overall, our method could cause a 1 %–5 % underestimation in  $p\text{CO}_2$ .

To reduce the artificial turbulence induced by anchored chambers, we used a small unmanned boat in the measurement, which allowed us to deploy drifting chambers freely in rivers deeper than 0.2 m and with a high flow velocity up to  $2 \text{ m s}^{-1}$ . During the deployment,  $\text{CO}_2$  emissions were determined using a circular 8.5 L floating chamber with a water surface area of  $0.113 \text{ m}^2$ . The chamber walls were lowered about 2 cm into the water and mounted with a pneumatic rubber tire. The chamber was connected to an infrared Li-850  $\text{CO}_2/\text{H}_2\text{O}$  gas analyzer (Li-Cor, Inc, USA) in a floating storage box through polyurethane tubes for  $\text{CO}_2$  analysis. An unmanned boat connected to both the chamber and box with ropes was used to deploy them near the central line of the river. Once the entire setup reached its designated location, the readings on the Li-850 were recorded at 0.5 s intervals. During the entire measurement process, the box drifted freely with the current. The Li-850 was calibrated by the manufacturer before field trips. The rate of  $\text{CO}_2$  efflux ( $\text{FCO}_2$  in  $\text{mmol m}^{-2} \text{ d}^{-1}$ ) was calculated from the observed change rate of the mole fraction  $S$  ( $\text{ppm s}^{-1}$ ) using

$$\text{FCO}_2 = (S \cdot V/A) \cdot t_1 \cdot t_2, \quad (5)$$

where  $S$  is the slope of  $\text{CO}_2$  accumulation in the chamber ( $\mu\text{atm s}^{-1}$ ),  $V$  is chamber gas volume ( $\text{m}^3$ ),  $A$  is the chamber area ( $\text{m}^2$ ),  $t_1 = 8.64 \times 10^4 \text{ s d}^{-1}$  is the conversion factor from seconds to days, and  $t_2$  is a conversion factor from mole fraction (ppm) to concentration ( $\text{mmol m}^{-3}$ ) at in situ temperature ( $T$  in K) and atmospheric pressure ( $p$  in Pa), according to the ideal gas law:

$$t_2 = p / (8.31 \text{ J K}^{-1} \text{ mole}^{-1} \cdot T) \cdot 1000. \quad (6)$$

The gas transfer velocity ( $k$ ) was calculated from  $\text{FCO}_2$  and  $p\text{CO}_2$  in both water and ambient air using

$$k = \text{FCO}_2 / \left( K_0 \cdot \left( p\text{CO}_2^{\text{water},i} - p\text{CO}_2^{\text{air}} \right) \right). \quad (7)$$

To compare gas transfer velocity values among different sites,  $k$  was standardized to  $k_{600}$  as described by Alin et al. (2011) using

$$k_{600} = k(600/Sc)^{-0.5}, \quad (8)$$

where  $Sc$  is the Schmidt number, which is dependent on temperature ( $T$ ) in degrees Celsius (Wanninkhof, 1992):

$$Sc = 1911.1 - 118.11T + 3.4527T^2 - 0.4132T^3. \quad (9)$$

In total, 196 chamber measurements were conducted. In 19 out of 215 sample sites, the drifting chamber was unable to deploy due to shallow water or high flow velocity. Meanwhile, 8 out of 196  $k_{600}$  data with the air–water  $p\text{CO}_2$  gradient less than  $200 \mu\text{atm}$  were also excluded, as the error in these calculations could be considerable (Borges et al., 2004).

### 3 Results

#### 3.1 Physical and biochemical characteristics

The Dong River was characterized by substantial seasonal variations in hydrologic regimes (Fig. 2). Stream width in the wet season was 17.0% and 5.6% larger than that in the dry season for small and large rivers, respectively (Table S1). The discharge ranged 4 orders of magnitude from  $0.1 \text{ m}^3 \text{ s}^{-1}$  in the small headwater streams during the dry season to  $6690 \text{ m}^3 \text{ s}^{-1}$  in the main stem during the wet season (Fig. S1). Water temperature was higher in July and August ( $21.4\text{--}33$  and  $21\text{--}33.4^\circ$ , respectively) than that in January ( $8.1\text{--}22.2^\circ$ ), April ( $16.5\text{--}26.9^\circ$ ), and October ( $17.4\text{--}29.7^\circ$ ). pH varied from 6.38 to 8.14, with a mean of 7.08. There was no significant (independent sample  $t$  test,  $p > 0.05$ ) change in pH between wet and dry seasons.  $U_{10}$  based on all stream sites was higher in large rivers ( $0.86 \pm 0.91$  and  $1.43 \pm 1.58 \text{ m s}^{-1}$  in wet and dry seasons, respectively) than in small rivers ( $0.62 \pm 0.61$  and  $0.76 \pm 0.73 \text{ m s}^{-1}$  in wet and dry seasons, respectively).

The streams presented low alkalinity ranging from 225 to  $3025 \mu\text{mol L}^{-1}$ . Overall, lower alkalinity was observed in the wet season than in the dry season (Table 1). In small rivers, the alkalinity in the wet season ( $656 \pm 265 \mu\text{mol L}^{-1}$ ) was 21.1% lower than that in the dry season ( $831 \pm 460 \mu\text{mol L}^{-1}$ ), and the lowest alkalinity was observed in April ( $615 \pm 262 \mu\text{mol L}^{-1}$ ), which was 30.4% lower than in January ( $883 \pm 548 \mu\text{mol L}^{-1}$ ). Similarly, the alkalinity in large rivers was  $790 \pm 402 \mu\text{mol L}^{-1}$  in the wet season, 14.5% lower than  $924 \pm 411 \mu\text{mol L}^{-1}$  in the dry season. However, the lowest value of alkalinity in large rivers was observed in August ( $739 \pm 312 \mu\text{mol L}^{-1}$ ) instead of April in small rivers.

Spatial and seasonal changes in DOC concentration were also observed in the surveyed rivers (Table 1).

DOC concentration in large rivers ( $1.94 \pm 1.52 \text{ mg L}^{-1}$ ) was 41.6% higher than that in small rivers ( $1.37 \pm 0.72 \text{ mg L}^{-1}$ ). Meanwhile, DOC concentrations in the wet season were  $2.22 \pm 1.82$  and  $1.54 \pm 0.72 \text{ mg L}^{-1}$  for large and small rivers, respectively, which were 45.1% and 54% higher than that in the dry season ( $1.53 \pm 0.72$  and  $1.11 \pm 0.63 \text{ mg L}^{-1}$  for large and small rivers, respectively).

#### 3.2 Spatial and seasonal variations in $p\text{CO}_2$

The  $p\text{CO}_2$  ranged from 15 to  $6323 \mu\text{atm}$  with a catchment-wide average of  $1748 \mu\text{atm}$  and showed considerable temporal and spatial variations throughout the sampling period. There was an increasing trend of observed  $p\text{CO}_2$  from small to large rivers (Fig. 3a). On average, the  $p\text{CO}_2$  values were  $856 \pm 444$ ,  $1481 \pm 979$ ,  $1354 \pm 753$ ,  $2332 \pm 1330$ ,  $2142 \pm 1016$ ,  $2271 \pm 1121$ , and  $2168 \pm 1046 \mu\text{atm}$  for streams from the first to seventh orders, respectively. The stronger increase in  $p\text{CO}_2$  occurred between third- and fourth-order streams (from  $1354 \pm 753$  to  $2332 \pm 1330 \mu\text{atm}$ , Fig. 3a). Overall,  $p\text{CO}_2$  in large rivers ( $2250 \pm 1178 \mu\text{atm}$ ) was 76.3% higher than that in small rivers ( $1276 \pm 796 \mu\text{atm}$ ). Meanwhile, there was also an increasing trend of  $p\text{CO}_2$  from rivers in the UDJRB compared with those in the LDJRB. The  $p\text{CO}_2$  values were  $2105 \pm 959$  and  $2487 \pm 1276 \mu\text{atm}$  for small and large rivers, respectively, in the LDJRB, which were 146.7% and 70% higher than that in the UDJRB, respectively (Fig. 3b).

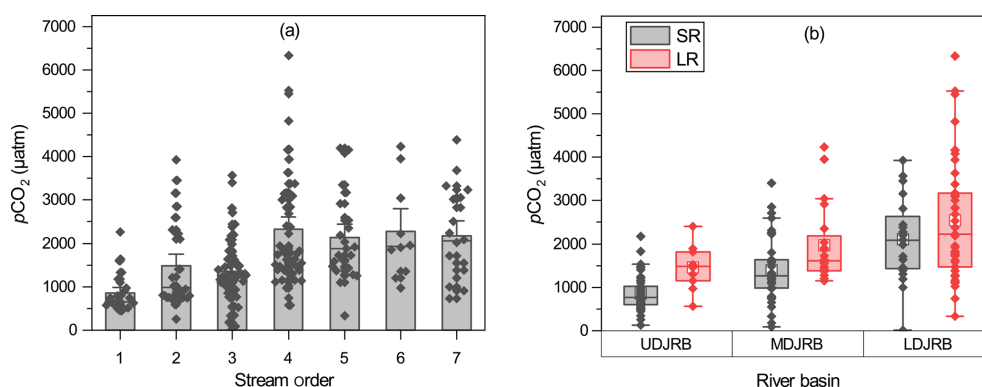
Seasonal variations in  $p\text{CO}_2$  differed across the stream size spectrum (Fig. 4). In small rivers, the highest  $p\text{CO}_2$  was observed in April ( $1506 \pm 880 \mu\text{atm}$ ), which was 50.3% higher compared with January ( $1002 \pm 660 \mu\text{atm}$ ).  $p\text{CO}_2$  then decreased in July ( $1131 \pm 589 \mu\text{atm}$ ) and increased in August ( $1325 \pm 863 \mu\text{atm}$ ) and October ( $1414 \pm 900 \mu\text{atm}$ ). Compared with small rivers, the peak of  $p\text{CO}_2$  in large rivers occurred later but persisted for a longer period of time. In large rivers, an increase in  $p\text{CO}_2$  was not observed until July.  $p\text{CO}_2$  in April was  $1831 \pm 793 \mu\text{atm}$ , which was similar to  $1805 \pm 1010 \mu\text{atm}$  in January, and it increased 39.3% to  $2550 \pm 1210 \mu\text{atm}$  in July.  $p\text{CO}_2$  peaked in August ( $2885 \pm 1351 \mu\text{atm}$ ) and then decreased to  $2176 \pm 1166 \mu\text{atm}$  in October. Overall,  $p\text{CO}_2$  was 9.3% and 21.7% higher in the wet season than in the dry season for small and large rivers, respectively.

#### 3.3 $\text{CO}_2$ effluxes and $k_{600}$

$\text{CO}_2$  effluxes ranged from  $-129.8$  to  $3874.8 \text{ mmol m}^{-2} \text{ d}^{-1}$  with a mean of  $225.2 \text{ mmol m}^{-2} \text{ d}^{-1}$ . More than 95% of the 196 samples had positive  $\text{FCO}_2$  values, indicating that a majority of the surveyed rivers are a carbon source. Overall, we observed higher  $\text{FCO}_2$  during the wet season than during the dry season in both small and large rivers (Fig. 5a).  $\text{FCO}_2$  in small rivers and large rivers was  $264.2 \pm 410.0$  and  $300.1 \pm 511.7 \text{ mmol m}^{-2} \text{ d}^{-1}$ , respectively, during the wet

**Table 1.** Seasonal variations in physical and biochemical characteristics, expressed as mean  $\pm$  SD.

Stream size	Season	Month	Water temperature ( $^{\circ}$ )	pH	Alkalinity ( $\mu\text{mol L}^{-1}$ )	DOC ( $\text{mg L}^{-1}$ )
Small	Dry	Jan	14.3 $\pm$ 4.1	7.05 $\pm$ 0.31	883 $\pm$ 548	1.07 $\pm$ 0.37
	Wet	Apr	19.9 $\pm$ 1.9	7.19 $\pm$ 0.26	615 $\pm$ 262	1.51 $\pm$ 0.58
	Wet	Jul	25.7 $\pm$ 2.3	7.17 $\pm$ 0.27	676 $\pm$ 227	1.59 $\pm$ 0.97
	Wet	Aug	27.1 $\pm$ 3.0	7.13 $\pm$ 0.38	678 $\pm$ 308	1.51 $\pm$ 0.56
	Dry	Oct	21.5 $\pm$ 2.6	7.08 $\pm$ 0.23	778 $\pm$ 358	1.16 $\pm$ 0.82
Large	Dry	Jan	16.9 $\pm$ 5.5	7.00 $\pm$ 0.27	961 $\pm$ 409	1.70 $\pm$ 1.52
	Wet	Apr	22.1 $\pm$ 3.7	7.20 $\pm$ 0.27	890 $\pm$ 386	2.22 $\pm$ 1.65
	Wet	Jul	27.8 $\pm$ 2.9	6.92 $\pm$ 0.25	740 $\pm$ 305	1.97 $\pm$ 1.77
	Wet	Aug	28.9 $\pm$ 3.3	6.92 $\pm$ 0.26	739 $\pm$ 312	2.47 $\pm$ 2.04
	Dry	Oct	25.2 $\pm$ 3.1	7.13 $\pm$ 0.29	887 $\pm$ 331	1.37 $\pm$ 0.67

**Figure 3.** Spatial variations in  $p\text{CO}_2$ . (a) Yearly average  $p\text{CO}_2$  in the seven stream orders; standard errors (SE) are displayed by error bars. (b) Measured  $p\text{CO}_2$  in small and large rivers among three regions in the DJRB. The box mid-lines represent medians; the interquartile range (IQR) is represented by the top and bottom of the box, respectively; whiskers indicate the range of 1.5 IQR; the white square symbols represent means, and the other symbols represent  $p\text{CO}_2$  values for each sampled site.

season, which was 87.2 % and 123.1 % higher than that in the dry season ( $141.1 \pm 188.7$  and  $134.5 \pm 129.5 \text{ mmol m}^{-2} \text{ d}^{-1}$  for small and large rivers, respectively). No significant (independent sample  $t$  test,  $p > 0.05$ ) difference in  $\text{FCO}_2$  was observed between small and large rivers.

$k_{600}$  differed greatly between river size classes and among hydrological periods (Fig. 5b).  $k_{600}$  values in small rivers were on average significantly (independent sample  $t$  test,  $p < 0.001$ ) higher than that in large rivers. The mean values of  $k_{600}$  in small rivers were  $8.29 \pm 11.29 \text{ m d}^{-1}$  and  $4.90 \pm 3.82 \text{ m d}^{-1}$  for the wet season and dry seasons, respectively, which were 112.6 % and 70 % higher than that of large rivers ( $3.90 \pm 5.55 \text{ m d}^{-1}$  in the wet season and  $2.25 \pm 1.61 \text{ m d}^{-1}$  in the dry season).  $k_{600}$  values during the wet season were also significantly (independent sample  $t$  test,  $p < 0.05$ ) higher than that in the dry season.  $k_{600}$  increased 112.7 % and 118.2 % from the dry season to wet season in small and large rivers, respectively. However, comparisons between different phases in the same hydrological period (e.g., early, middle, and late wet season) did not dif-

fer significantly (paired sample  $t$  test,  $p > 0.05$ ) for both river size classes.

The spatial and temporal variations in  $\text{CO}_2$  efflux generally coincided with the changes in  $p\text{CO}_2$  and  $k_{600}$ . In small rivers, the highest  $\text{CO}_2$  effluxes were  $346.8 \pm 625.2 \text{ mmol m}^{-2} \text{ d}^{-1}$  during April, consistent with the high  $k_{600}$  and  $p\text{CO}_2$  in this period. In large rivers, high  $\text{CO}_2$  effluxes were observed in both April ( $339.9 \pm 828.6 \text{ mmol m}^{-2} \text{ d}^{-1}$ ) and August ( $329.9 \pm 270.0 \text{ mmol m}^{-2} \text{ d}^{-1}$ ), which were attributed to the concurrently high  $k_{600}$  in April and high  $p\text{CO}_2$ .

## 4 Discussions

### 4.1 Underlying processes of $p\text{CO}_2$ dynamics

The spatial pattern of  $p\text{CO}_2$  in the DJRB likely results from the changes in terrestrial carbon inputs (i.e., organic and inorganic carbon) and in-stream metabolism, both of which var-

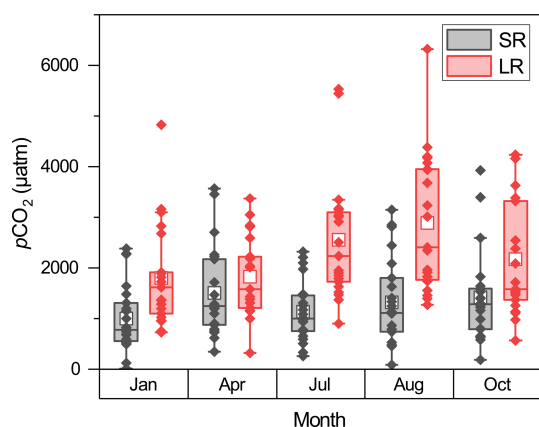


**Figure 4.** Seasonal  $p\text{CO}_2$  changes in small and large rivers. The box mid-lines represent medians; the interquartile range (IQR) is represented by the top and bottom of the box, respectively; whiskers indicate the range of 1.5 IQR; the white square symbols represent means, and the other symbols represent  $p\text{CO}_2$  values for each sampled site.

ied due to different land cover and catchment topography. The higher  $p\text{CO}_2$  values in large rivers than small rivers were associated with a higher percentage of urban and cropland cover and a lower forest cover (Fig. 6). Compared with forest, cropland could provide a more favorable condition for soil erosion and the transfer of terrestrial carbon from land to rivers, contributing to a higher  $p\text{CO}_2$ . Intensification of agricultural practices could promote the decomposition of soil organic matter (Borges et al., 2018), thereby increasing the concentration of  $\text{CO}_2$  and liable DOC in the soil (Borges et al., 2018). The soil  $\text{CO}_2$  could be easily transported to rivers and thus increase the  $p\text{CO}_2$ , while the liable DOC could be decomposed rapidly after entering the rivers due to their sensitivity to in-stream metabolism (Lambert et al., 2017; Li et al., 2019). Meanwhile, the input of wastewater with high organic matter concentration from urban areas could also contribute to an increase in riverine  $p\text{CO}_2$  (Xuan et al., 2020; Zhang et al., 2021). Our results showed increasing  $p\text{CO}_2$  from forest-dominated streams in the UDJRB relative to those in agricultural and urban-impacted catchments in the MDJRB and LDJRB (Fig. 3b). The  $>70\%$  forest cover in the UDJRB (Fig. 1) may have greatly reduced the soil erosion intensity (Ran et al., 2018). Meanwhile, the organic matter from forest tends to be more aromatic and thus more capable of surviving biodegradation (Kalbitz and Kaiser, 2008), leading to a relatively low riverine  $p\text{CO}_2$  value. In contrast, cropland, occupying about 49% of the land cover (Fig. 1), was the primary land use type in the MDJRB substituting forest, and urban areas account for  $\sim 17\%$  of the land cover in the LDJRB. The higher  $p\text{CO}_2$  in the MDJRB and LDJRB is likely under the influence of agricultural practices and wastewater input. Overall, land use mainly affects the spatial

distribution of  $p\text{CO}_2$  by altering the amount and lability of carbon inputs to the rivers.

Moreover, different catchment topography in small and large rivers may have also contributed to the differences in  $p\text{CO}_2$ . Due to steeper channel slopes and higher flow velocities, small rivers in the DJRB have higher  $k_{600}$  (Fig. 5b). As a consequence,  $\text{CO}_2$  in small rivers can exchange with the atmosphere more rapidly, preventing the build-up of dissolved  $\text{CO}_2$  and thus lower  $p\text{CO}_2$  (Rocher-Ros et al., 2019). Therefore, other processes have facilitated the carbon transfer from small rivers to downstream large rivers, sustaining the higher  $p\text{CO}_2$  in large rivers. Recent studies indicate that carbonate buffering could decrease the  $\text{CO}_2$  emissions from small rivers by increasing the ionization of  $\text{CO}_2$  (Stets et al., 2017), thereby increasing the transfer of DIC towards the rivers downstream, which resulted in the higher  $p\text{CO}_2$  in large downstream rivers. However, strong carbonate buffering usually occurs in high-alkalinity ( $>2500\ \mu\text{mol L}^{-1}$ ) streams with high pH ( $>8$ ), while in low-alkalinity waters, the pool of ionized  $\text{CO}_2$  is relatively small, indicating a weak carbonate buffering (Stets et al., 2017). Since the streams in the DJRB were characterized by low alkalinity ( $726 \pm 364$  and  $844 \pm 409\ \mu\text{mol L}^{-1}$  for small and large rivers, respectively), carbonate buffering is unlikely a primary contributor to the high  $p\text{CO}_2$  in large rivers. Meanwhile, our data showed that river water  $p\text{CO}_2$  was negatively related to DO and positively related to DOC (Fig. 7), suggesting that the high  $p\text{CO}_2$  in large rivers was related to metabolic processes. The steep channel slopes in small rivers tend to promote the transfer of OC to downstream large rivers. As a consequence, it is difficult for terrestrial organic carbon to be converted into  $\text{CO}_2$  in small rivers due to the short water residence time (Hotchkiss et al., 2015). Conversely, a greater fraction of OC may have been transported downstream and fuel the heterotrophic respiration in large rivers, where low flow velocity and long water residence time facilitated the decomposition of organic carbon within the water column (Denfeld et al., 2013).

To compare the contribution of internal metabolism and external  $\text{CO}_2$  input on  $p\text{CO}_2$  in small and large rivers, the  $\Delta\text{CO}_2 : \Delta\text{O}_2$  stoichiometry was used to evaluate the impacts of respiration and photosynthesis processes on the concentration of dissolved  $\text{O}_2$  and  $\text{CO}_2$  (Stets et al., 2017). The inverse relation between  $\Delta\text{CO}_2$  and  $\Delta\text{O}_2$  (Fig. 8) demonstrated that metabolic processes are important for the dissolved  $\text{CO}_2$  concentration variations (Amaral et al., 2020), while the difference in the  $\Delta\text{CO}_2 : \Delta\text{O}_2$  stoichiometry between small and large rivers suggested the different strength of in-stream metabolism (Rasera et al., 2013). The  $\Delta\text{CO}_2 : \Delta\text{O}_2$  stoichiometry in large rivers is closer to the 1 : 1 line than that in small rivers, indicating that large rivers are more affected by the metabolic processes (Jeffrey et al., 2018; Amaral et al., 2020). For large rivers, the linear regression is  $\Delta\text{CO}_2 = -0.999 (\pm 0.081) \Delta\text{O}_2 + 18.020 (\pm 5.995)$  ( $r^2 = 0.62$ ,  $p < 0.001$ ). When the  $\text{CO}_2$  concentration increases in

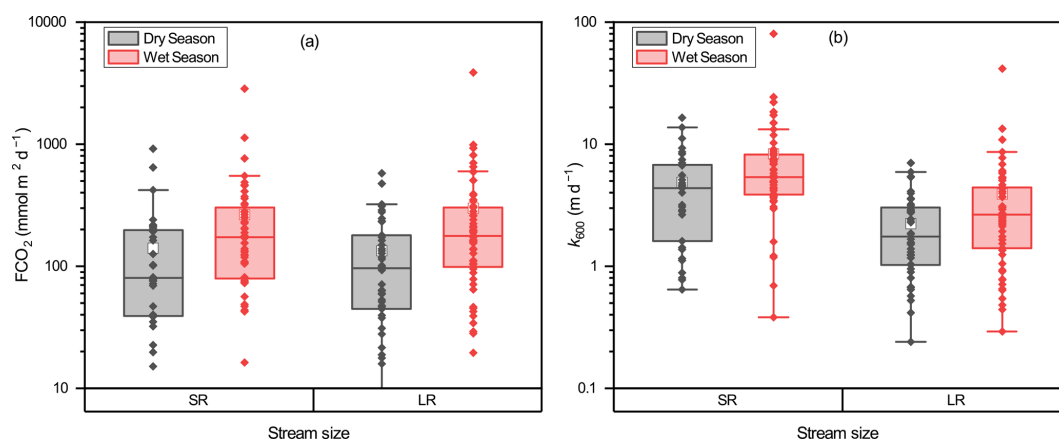


**Figure 5.** Relationship between stream size and (a)  $\text{FCO}_2$  and (b)  $k_{600}$ . The box mid-lines represent medians; the interquartile range (IQR) is represented by the top and bottom of the box, respectively; whiskers indicate the range of 1.5 IQR; the white square symbols represent means, and the other symbols represent  $\text{FCO}_2$  and  $k_{600}$  values for each sampled site.

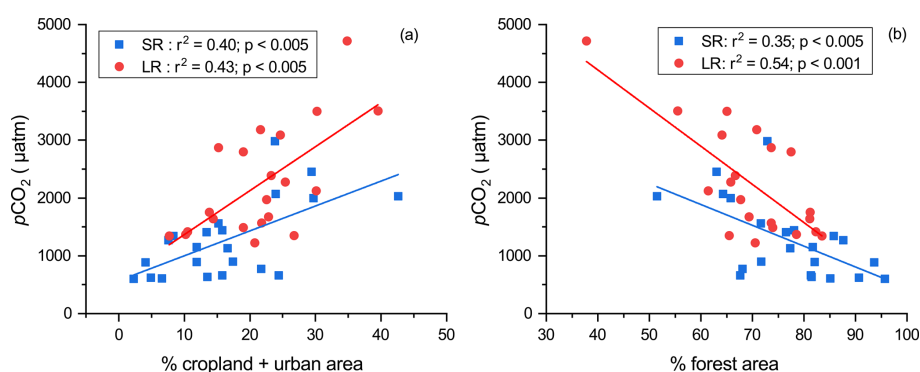


**Figure 6.** (a) The relationship between yearly average  $p\text{CO}_2$  at each site and the percentage of cropland and urban area combined; (b) the relationship between yearly average  $p\text{CO}_2$  at each site and the percentage of forest area.

large rivers, a similar magnitude of decrease in dissolved  $\text{O}_2$  concentration occurs, indicating that in-stream metabolism is the primary control on  $p\text{CO}_2$ . In contrast, the linear regression for small rivers is  $\Delta\text{CO}_2 = -0.868 (\pm 0.098) \Delta\text{O}_2 + 21.42 (\pm 4.175)$  ( $r^2 = 0.41$ ,  $p < 0.001$ ), which means that with the  $\text{CO}_2$  concentration increasing by  $1 \mu\text{mol L}^{-1}$ , the  $\text{O}_2$  concentration decreases by only  $0.868 \mu\text{mol L}^{-1}$ . Therefore, extra  $\text{CO}_2$  inputs have contributed to the changes in  $p\text{CO}_2$  despite the strong presence of in-stream metabolism.

On the other hand, the temporal pattern was affected by precipitation and temperature seasonality. Our results showed that higher  $p\text{CO}_2$  occurred in the wet season than in the dry season for both small and large rivers (Fig. 4). The elevated temperature in the wet season could promote a substantial increase in the net primary productivity of the terrestrial ecosystem, while increased precipitation can facilitate the transfer of terrestrial carbon (Rasera et al., 2013), including both soil  $\text{CO}_2$  and OC, from land to rivers. This could either directly increase riverine  $p\text{CO}_2$  or fuel OC decomposition (Borges et al., 2018). However, the differences

in seasonal changes of  $p\text{CO}_2$  between small and large rivers (Fig. 4) also suggested that their controlling process could be different. For small rivers, the highest  $p\text{CO}_2$  value was observed in April (Fig. 4), which is consistent with the rapid surge of terrestrial C inputs, usually occurring at the onset of the wet season (Hope et al., 2004; Yao et al., 2007; Johnson et al., 2008). However, such increase in  $p\text{CO}_2$  was not observed in large rivers (Fig. 4), though the DOC in large rivers increased at a rate similar to that in small rivers during the same period (Table 1). A possible explanation is that the observed  $p\text{CO}_2$  rise mainly originated from soil  $\text{CO}_2$ , which was readily emitted from the small rivers into the air, with little reaching the larger rivers downstream (Denfeld et al., 2013; Drake et al., 2018). Differences in the  $p\text{CO}_2$  dynamics in July and August also reflected different controlling processes in small and large rivers. A decline in  $p\text{CO}_2$  in July in small rivers suggested that it might have experienced the depletion effect occurring in the middle and late wet season (Hope et al., 2004), during which soil  $\text{CO}_2$  decreased due to the continual precipitation. In contrast, the increase in  $p\text{CO}_2$

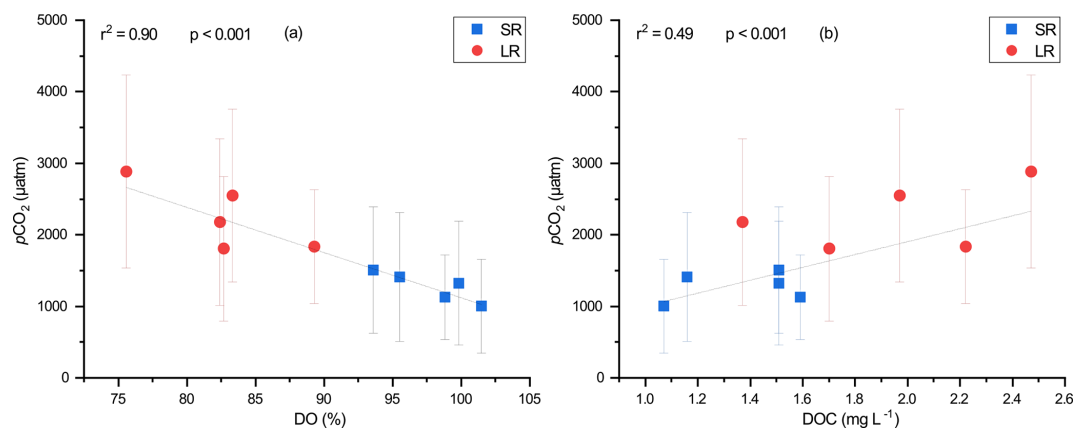


**Figure 7.** Relationship between seasonal average  $p\text{CO}_2$  and (a) DO and (b) DOC. Error bars for the  $p\text{CO}_2$  represent 1 standard deviation from the seasonal mean. The DO– $p\text{CO}_2$  and DOC– $p\text{CO}_2$  relationships are shown as solid lines.

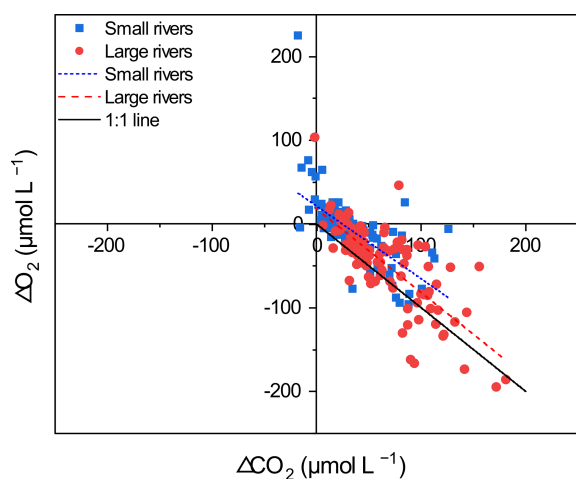


**Figure 8.** The relationship between  $\Delta\text{CO}_2$  and  $\Delta\text{O}_2$ . Points greater than zero are oversaturated, and points less than zero are undersaturated. Points above the 1 : 1 line indicate the existence of additional carbon sources, apart from in-stream metabolic processes. For large rivers, the linear regression is  $\Delta\text{CO}_2 = -0.999 (\pm 0.081) \Delta\text{O}_2 + 18.020 (\pm 5.995)$  ( $r^2 = 0.62$ ,  $p < 0.001$ ). For small rivers, the linear regression is  $\Delta\text{CO}_2 = -0.868 (\pm 0.098) \Delta\text{O}_2 + 21.42 (\pm 4.175)$  ( $r^2 = 0.41$ ,  $p < 0.001$ ).

in large rivers in July indicated that the decreased soil  $\text{CO}_2$  inputs could hardly affect the  $p\text{CO}_2$  in large rivers during this period. Instead, stronger in-stream metabolism caused by OC inputs and the favorable conditions for OC decomposition are more likely to be responsible for the rising  $p\text{CO}_2$ . In addition, there are other processes that may have affected the riverine  $p\text{CO}_2$ . For example, stronger solar radiation during summer could increase photo-oxidation in rivers. However, the commonly observed lower daytime  $\text{CO}_2$  emission rates than nocturnal rates (Gómez-Gener et al., 2021) suggest that photosynthesis overrides photo-oxidation in  $\text{CO}_2$  dynamics. Nonetheless, the low DO concentration observed

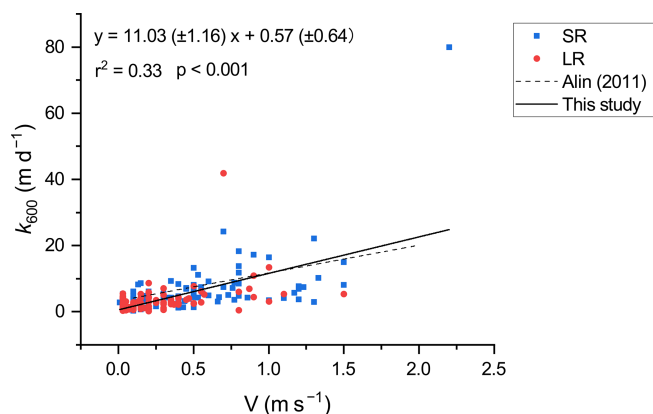
in the surveyed rivers (Fig. 8) suggested that photosynthesis is not likely the primary control on the seasonal variation in  $p\text{CO}_2$ .

#### 4.2 Environmental control of $k_{600}$ variation

Environmental factors, including wind speed and hydrological variables, could affect the gas exchange at the water–air interface and are typically used to explain the variance in  $k_{600}$  (Alin et al., 2011; Raymond et al., 2012). Flow velocity generally determines the  $k_{600}$  in small rivers, while wind speed becomes a more important factor in controlling the  $k_{600}$  in large rivers, reservoirs, and estuaries (Guérin et al., 2007; Rasera et al., 2013; Amaral et al., 2020). In our surveyed rivers,  $k_{600}$  displayed a significant linear correlation (Pearson correlation,  $p < 0.001$ ) with the flow velocity. Our  $k_{600}$  model (Fig. 9) based on 188 field measurement data is similar to that developed by Alin et al. (2011) ( $k_{600} = 13.82 + 0.35v$ ). However, in our studied rivers, no significant correlation (Pearson correlation  $p > 0.05$ ) was found between wind speed and  $k_{600}$  regardless of stream size. This could be explained by the lower wind speed ( $0.68 \pm 0.66$  and  $1.09 \pm 1.06 \text{ m s}^{-1}$  for small and large rivers, respectively; Table 2) (Guérin et al., 2007). As the wind speed decreases, the impact of flow velocity on  $k_{600}$  becomes increasingly predominant (Borges et al., 2004). Therefore, the accuracy of  $k_{600}$  estimation based on wind speed in nearby regions should be examined using measurement data (Yao et al., 2007; Li et al., 2018). The temporal heterogeneities of  $k_{600}$  between small and large rivers reveal the differences in flow regime. The  $k_{600}$  values in small rivers are significantly higher than that in large rivers (independent sample  $t$  test,  $p < 0.001$ ), which could be explained by the higher flow velocity in small rivers. Meanwhile, the significantly higher  $k_{600}$  in the wet season than in the dry season (independent sample  $t$  test,  $p < 0.05$ ) is the result of the increased flow velocity and turbulence due to monsoon-

**Table 2.** Seasonal variation in  $k_{600}$  and environmental factors in small and large rivers.

Stream size	Season	Current velocity ( $\text{m s}^{-1}$ )	$U_{10}$ ( $\text{m s}^{-1}$ )	$k_{600}$ ( $\text{m d}^{-1}$ )
Small	Wet	$0.66 \pm 0.47$	$0.62 \pm 0.61$	$8.29 \pm 11.29$
	Dry	$0.43 \pm 0.27$	$0.76 \pm 0.73$	$4.90 \pm 3.82$
Large	Wet	$0.32 \pm 0.32$	$0.86 \pm 0.91$	$3.90 \pm 5.55$
	Dry	$0.17 \pm 0.19$	$1.43 \pm 1.58$	$2.25 \pm 1.61$

**Figure 9.** Relationship between  $k_{600}$  and flow velocity. The dashed line represents the parameterization of Alin et al. (2011).

induced precipitation during the wet season (Guérin et al., 2007; Alin et al., 2011; Ho et al., 2018).

Exceptionally high  $k_{600}$  values were observed in the surveyed rivers (Fig. 9). The highest  $k_{600}$  values in large and small rivers were  $41.83$  and  $79.97 \text{ m d}^{-1}$ , respectively, which were 5-fold and 3-fold larger than calculated  $k_{600}$ , respectively. This is likely the result of the exponential increase in  $k_{600}$  due to extreme flood events. Generally, flood events associated with heavy rainfall can substantially increase flow velocity and near-surface turbulence (Almeida et al., 2017; Geeraert et al., 2017), leading to extremely high  $k_{600}$  values. Yet, neither our model nor the one from Alin et al. (2011) was suitable for the estimation of  $k_{600}$  during extreme flood events because the calculated  $k_{600}$  could deviate far from the measured  $k_{600}$  when they occurred. The extent to which flood events affect  $k_{600}$  and riverine  $\text{CO}_2$  emission is still uncertain and warrant continued research (Drake et al., 2018).

### 4.3 A comparison of $\text{CO}_2$ emissions to other rivers

The mean  $\text{CO}_2$  fluxes of  $225.2 \text{ mmol m}^{-2} \text{ d}^{-1}$  in the DJRB are comparable to those observed in tropical and subtropical rivers in the Americas, Africa, and Southeast Asia (Table 3). Although the magnitude of the  $\text{CO}_2$  emissions of these river systems is similar, the seasonal variations and drivers behind them could differ. The  $\text{CO}_2$  emissions from the Dong

River were higher in the wet season than in the dry season. This seasonal pattern is similar to that observed in the Xi and Daning rivers (Yao et al., 2007; Ni et al., 2019) but different from that observed in the Jinshui River in the upper Yangtze River, where  $p\text{CO}_2$  is high in winter and low in summer (Luo et al., 2019), although all four rivers are in the East Asian Monsoon climate region. The seasonal differences in  $\text{CO}_2$  emissions are largely caused by the  $p\text{CO}_2$  variability, which in turn is regulated by external carbon inputs, internal production of  $\text{CO}_2$  (Yao et al., 2007), and the dilution effect caused by precipitation (Johnson et al., 2007). For rivers where  $p\text{CO}_2$  is lower in summer than in winter, the dilution effect overrides the effect of increased carbon inputs and internal  $\text{CO}_2$  production (Luo et al., 2019). In contrast, for rivers like the Dong River, although the dilution effect remains, increased  $\text{CO}_2$  inputs and metabolism are more significant factors in controlling its  $p\text{CO}_2$ , thus leading to higher summer  $p\text{CO}_2$ . In addition, the controlling processes of the Dong River could be different even when compared with rivers with similar seasonal variations in the same climatic zone. For instance, the DO in the Xi River was supersaturated, indicating that its aquatic photosynthetic activities predominated aquatic metabolism and tended to reduce its  $\text{CO}_2$  concentration (Yao et al., 2007). Therefore, other carbon sources like soil respiration and carbonate weathering should be responsible for the high  $p\text{CO}_2$  in summer (Zhang et al., 2019). In contrast, the low DO value and the negative correlation between DO and  $p\text{CO}_2$  in the Dong River indicated that photosynthesis is relatively weak compared with the respiration, and the latter process is an essential source of riverine  $\text{CO}_2$  (Stets et al., 2017), resulting in a higher  $p\text{CO}_2$  in summer.

The  $\text{CO}_2$  fluxes in small rivers are similar to those in large rivers, which is contradictory to the finding in previous studies that  $\text{CO}_2$  effluxes should be higher in small rivers than in large rivers due to the input of  $\text{CO}_2$ -rich groundwater (Duvert et al., 2018). The depletion and diffusion effect may be responsible for the discrepancy (Johnson et al., 2007; Dinsmore et al., 2013). Groundwater in the DJRB could be easily diluted due to abundant monsoon-induced rainfall, preventing it from supplying the small rivers with high  $\text{CO}_2$  concentrations. However, we recognize that the impact of groundwater on  $p\text{CO}_2$  in small rivers may be overlooked in our

**Table 3.** Comparison of  $\text{CO}_2$  emissions from subtropical and tropical rivers.

Rivers	Climate	Season	$p\text{CO}_2$ ( $\mu\text{atm}$ )	$k_{600}$ ( $\text{m d}^{-1}$ )	$\text{FCO}_2$ ( $\text{mmol m}^{-2} \text{d}^{-1}$ )	References
The Dong River (large rivers)	Subtropical	Wet	$2422 \pm 1209$	$3.90 \pm 5.55$	$300.1 \pm 511.8$	This study
		Dry	$1990 \pm 1094$	$2.25 \pm 1.61$	$134.5 \pm 129.5$	
The Dong River (small rivers)		Wet	$1321 \pm 792$	$8.29 \pm 11.29$	$264.2 \pm 410.0$	
		Dry	$1191 \pm 825$	$4.90 \pm 3.82$	$129.5 \pm 197.2$	
The Xi River (mainstream)	Subtropical		2600		190.3–358.6	Yao et al. (2007)
The lower Mekong River	Tropical		$1090 \pm 290$	6.24 <sup>a</sup>	194.5	Li et al. (2013)
The Yangtze River (Jinshui River) (headwater stream)	Subtropical		$1147 \pm 874$	$11.1 \pm 4.5^a$	$343 \pm 413$	Luo et al. (2019)
		Dry	$1562 \pm 975$		$542 \pm 477$	
		Wet	$834 \pm 639$		$192 \pm 278$	
The upper Yangtze River (Daning River)	Subtropical		$1198.2 \pm 1122.9$		$329.8 \pm 470.2$	Ni et al. (2019)
		Rainy	$1243.7 \pm 1111.5$	$8.1\text{--}14.1^a$	$357.4 \pm 483.7$	
		Dry	$1145.5 \pm 1146.2$	$7.0\text{--}8.8^a$	$288.7 \pm 450.0$	
The Zambezi River	Tropical	Wet	$3102.5^b$	$0.05\text{--}1.51$	350.75	Teodoru et al. (2015)
		Dry	$1150^b$		51.92	
The Congo River	Tropical	High water	$6001 \pm 5008$		1149 or 1520	Borges et al. (2015a, b)
		Low water	$4867 \pm 2578$			
		Falling water	$5321 \pm 3383$			
The lower Red River	Tropical		$1589 \pm 43$	$12.22 \pm 6.48$	$530.3 \pm 16.9$	Le et al. (2018)
Caboolture River	Subtropical		$3000 \pm 33$		$379 \pm 53$	Jeffrey et al. (2018)
Rajang River	Tropical	Wet	$2531 \pm 188$	$0.55\text{--}2.93$	141.67	Müller-Dum et al. (2019)
		Dry	$2337 \pm 304$		125	
Lower Mississippi River	Subtropical		$1514 \pm 652$		172.8	Reiman and Xu (2019b)
Amazonian rivers	Tropical		259–7808	5.06	69.12–1321.92	Rasera et al. (2013)

<sup>a</sup>  $k$  values were shown here because  $k_{600}$  values were not provided in references. <sup>b</sup> The unit for  $p\text{CO}_2$  is ppm.

sampling process since the  $\text{CO}_2$  carried by groundwater can emit into the atmosphere within a very short distance (Duvert et al., 2018). In view of the above, it is recommended that further studies targeting the release of groundwater  $\text{CO}_2$  to the atmosphere be carried out in the future.

## 5 Conclusions

Studying  $\text{CO}_2$  emissions from subtropical rivers is an essential step toward more accurate estimates of global  $\text{CO}_2$  emissions from river systems. By deploying floating chambers, seasonal changes in riverine  $p\text{CO}_2$  and  $\text{CO}_2$  emissions from the Dong River catchment were investigated. Spatial and temporal patterns of  $p\text{CO}_2$  were mainly affected by terrestrial carbon inputs (i.e., organic and inorganic carbon) and in-stream metabolism, both of which varied due to different land cover, catchment topography, and seasonality of precip-

itation and temperature.  $k_{600}$  was higher in small rivers than in large rivers and higher during the wet season than during the dry season, both of which can be explained by the observed significant correlation between  $k_{600}$  and flow velocity. In contrast to previous studies, similar  $\text{CO}_2$  fluxes were observed among small and large rivers in the DJRB. It is suggested that the absence of commonly observed higher  $\text{CO}_2$  fluxes in small rivers could be associated with the depletion effect caused by abundant and persistent precipitation in this subtropical monsoon catchment. There is no doubt that the spatial and temporal variations in  $\text{CO}_2$  emissions from the DJRB reflected the complexity and diversity of controlling factors. As a step towards a more accurate estimate of the carbon budget in the catchment, comprehensive and systematic measurements of  $\text{CO}_2$  emissions covering a broad range of stream sizes and seasons are of paramount importance.

**Data availability.**  $\text{CO}_2$  emission data used in this study are available online at <https://doi.org/10.25442/hku.13416281.v1> (Liu, 2020). Other data are available from the corresponding author Lishan Ran upon request at [lsran@hku.hk](mailto:lsran@hku.hk).

**Supplement.** The supplement related to this article is available online at: <https://doi.org/10.5194/bg-18-5231-2021-supplement>.

**Author contributions.** BL and LR conceived the study. BL, MT, CNC, XY, and LR carried out the fieldwork. BL, MT, and KS designed and performed the laboratory analysis. BL composed the manuscript with contributions from all authors.

**Competing interests.** The authors declare that they have no conflict of interest.

**Disclaimer.** Publisher's note: Copernicus Publications remains neutral with regard to jurisdictional claims in published maps and institutional affiliations.

**Acknowledgements.** We thank Steven Bouillon and the two anonymous reviewers for their constructive comments which have greatly improved the paper.

**Financial support.** This research has been supported by the Research Grants Council of Hong Kong (grant nos. 17300619 and 27300118) and the National Natural Science Foundation of China (grant no. 41807318). This research has also been supported by the Hui Oi-Chow Trust Fund (grant no.201801172006).

**Review statement.** This paper was edited by Steven Bouillon and reviewed by two anonymous referees.

## References

- Abril, G., Martinez, J. M., Artigas, L. F., Moreira-Turcq, P., Benedetti, M. F., Vidal, L., Meziane, T., Kim, J. H., Bernardes, M. C., Savoye, N., Deborde, J., Souza, E. L., Alberic, P., Landim de Souza, M. F., and Roland, F.: Amazon River carbon dioxide outgassing fuelled by wetlands, *Nature*, 505, 395–398, <https://doi.org/10.1038/nature12797>, 2014.
- Abril, G., Bouillon, S., Darchambeau, F., Teodoru, C. R., Marwick, T. R., Tamooh, F., Ochieng Omengo, F., Geeraert, N., Deirmendjian, L., Polsenaere, P., and Borges, A. V.: Technical Note: Large overestimation of  $p\text{CO}_2$  calculated from pH and alkalinity in acidic, organic-rich freshwaters, *Biogeosciences*, 12, 67–78, <https://doi.org/10.5194/bg-12-67-2015>, 2015.
- Alin, S. R., Rasera, M. d. F. F. L., Salimon, C. I., Richey, J. E., Holtgrieve, G. W., Krusche, A. V., and Snidvongs, A.: Physical controls on carbon dioxide transfer velocity and flux in low-gradient river systems and implications for regional carbon budgets, *J. Geophys. Res.*, 116, G01009, <https://doi.org/10.1029/2010jg001398>, 2011.
- Almeida, R. M., Pacheco, F. S., Barros, N., Rosi, E., and Roland, F.: Extreme floods increase  $\text{CO}_2$  outgassing from a large Amazonian river, *Limnol. Oceanogr.*, 62, 989–999, <https://doi.org/10.1002/lno.10480>, 2017.
- Amaral, J. H. F., Melack, J. M., Barbosa, P. M., MacIntyre, S., Kasper, D., Cortés, A., Silva, T. S. F., Nunes de Sousa, R., and Forsberg, B. R.: Carbon dioxide fluxes to the atmosphere from waters within flooded forests in the Amazon basin, *J. Geophys. Res.-Biogeo.*, 125, e2019JG005293, <https://doi.org/10.1029/2019JG005293>, 2020.
- Battin, T. J., Luysaert, S., Kaplan, L. A., Aufdenkampe, A. K., Richter, A., and Tranvik, L. J.: The boundless carbon cycle, *Nat. Geosci.*, 2, 598–600, <https://doi.org/10.1038/ngeo618>, 2009.
- Borges, A. V., Delille, B., Schiettecatte, L. S., Gazeau, F., Abril, G., Frankignoulle, M. J. L., and Oceanography: Gas transfer velocities of  $\text{CO}_2$  in three European estuaries (Randers Fjord, Scheldt, and Thames), *Limnol. Oceanogr.*, 49, 1630–1641, <https://doi.org/10.4319/lo.2004.49.5.1630>, 2004.
- Borges, A. V., Abril, G., Darchambeau, F., Teodoru, C. R., Deborde, J., Vidal, L. O., Lambert, T., and Bouillon, S.: Divergent biophysical controls of aquatic  $\text{CO}_2$  and  $\text{CH}_4$  in the World's two largest rivers, *Sci. Rep.*, 5, 15614, <https://doi.org/10.1038/srep15614>, 2015a.
- Borges, A. V., Darchambeau, F., Teodoru, C. R., Marwick, T. R., Tamooh, F., Geeraert, N., Omengo, F. O., Guérin, F., Lambert, T., Morana, C., Okuku, E., and Bouillon, S.: Globally significant greenhouse-gas emissions from African inland waters, *Nat. Geosci.*, 8, 637–642, <https://doi.org/10.1038/ngeo2486>, 2015b.
- Borges, A. V., Darchambeau, F., Lambert, T., Bouillon, S., Morana, C., Brouyere, S., Hakoun, V., Jurado, A., Tseng, H. C., Descy, J. P., and Roland, F. A. E.: Effects of agricultural land use on fluvial carbon dioxide, methane and nitrous oxide concentrations in a large European river, the Meuse (Belgium), *Sci. Total Environ.*, 610/611, 342–355, <https://doi.org/10.1016/j.scitotenv.2017.08.047>, 2018.
- Chen, Q., Xu, W., Li, S., Fu, S., and Yan, J.: Aboveground biomass and corresponding carbon sequestration ability of four major forest types in south China, *Chin. Sci. Bull.*, 58, 1551–1557, <https://doi.org/10.1007/s11434-012-5100-8>, 2013.
- Chen, Y. D., Zhang, Q., Lu, X., Zhang, S., and Zhang, Z.: Precipitation variability (1956–2002) in the Dongjiang River (Zhujiang River basin, China) and associated large-scale circulation, *Quaternary Int.*, 244, 130–137, <https://doi.org/10.1016/j.quaint.2010.08.013>, 2011.
- Cole, J. J., Prairie, Y. T., Caraco, N. F., McDowell, W. H., Tranvik, L. J., Striegl, R. G., Duarte, C. M., Kortelainen, P., Downing, J. A., Middelburg, J. J., and Melack, J.: Plumbing the global carbon cycle: Integrating inland waters into the terrestrial carbon budget, *Ecosystems*, 10, 172–185, <https://doi.org/10.1007/s10021-006-9013-8>, 2007.
- Denfeld, B. A., Frey, K. E., Sobczak, W. V., Mann, P. J., and Holmes, R. M.: Summer  $\text{CO}_2$  evasion from streams and rivers in the Kolyma River basin, north-east Siberia, *Polar Res.*, 32, 19704, <https://doi.org/10.3402/polar.v32i0.19704>, 2013.

- Dickson, A. G., Sabine, C. L., and Christian, J. R. (Eds.): Guide to Best Practices for Ocean  $\text{CO}_2$  Measurements, North Pacific Marine Science Organization, BC, Canada, 2007.
- Ding, J., Jiang, Y., Fu, L., Liu, Q., Peng, Q., and Kang, M.: Impacts of land use on surface water quality in a subtropical river basin: A case study of the Dongjiang River Basin, Southeastern China, *Water*, 7, 4427–4445, <https://doi.org/10.3390/w7084427>, 2015.
- Dinsmore, K. J., Wallin, M. B., Johnson, M. S., Billett, M. F., Bishop, K., Pumpanen, J., and Ojala, A.: Contrasting  $\text{CO}_2$  concentration discharge dynamics in headwater streams: A multi-catchment comparison, *J. Geophys. Res.-Biogeo.*, 118, 445–461, <https://doi.org/10.1002/jgrg.20047>, 2013.
- Drake, T. W., Raymond, P. A., and Spencer, R. G.: Terrestrial carbon inputs to inland waters: A current synthesis of estimates and uncertainty, *Limnol. Oceanogr. Lett.*, 3, 132–142, <https://doi.org/10.1002/lol2.10055>, 2018.
- Duvert, C., Butman, D. E., Marx, A., Ribolzi, O., and Hutley, L. B.:  $\text{CO}_2$  evasion along streams driven by groundwater inputs and geomorphic controls, *Nat. Geosci.*, 11, 813–818, <https://doi.org/10.1038/s41561-018-0245-y>, 2018.
- Fu, Y., Tang, C., Li, J., Zhao, Y., Zhong, W., and Zeng, X.: Sources and transport of organic carbon from the Dongjiang River to the Humen outlet of the Pearl River, southern China, *J. Geogr. Sci.*, 24, 143–158, <https://doi.org/10.1007/s11442-014-1078-2>, 2014.
- Geeraert, N., Omengo, F. O., Borges, A. V., Govers, G., and Bouillon, S.: Shifts in the carbon dynamics in a tropical lowland river system (Tana River, Kenya) during flooded and non-flooded conditions, *Biogeochemistry*, 132, 141–163, <https://doi.org/10.1007/s10533-017-0292-2>, 2017.
- Gómez-Gener, L., Rocher-Ros, G., Battin, T., Cohen, M. J., Dalmagro, H. J., Dinsmore, K. J., Drake, T. W., Duvert, C., Enrich-Prast, A., Horgby, Å., Johnson, M. S., Kirk, L., Machado-Silva, F., Marzolf, N. S., McDowell, M. J., McDowell, W. H., Miittinen, H., Ojala, A. K., Peter, H., Pumpanen, J., Ran, L., Riveros-Iregui, D. A., Santos, I. R., Six, J., Stanley, E. H., Wallin, M. B., White, S. A., and Sponseller, R. A.: Global carbon dioxide efflux from rivers enhanced by high nocturnal emissions, *Nat. Geosci.*, 14, 289–294, <https://doi.org/10.1038/s41561-021-00722-3>, 2021.
- Guérin, F., Abril, G., Serça, D., Delon, C., Richard, S., Delmas, R., Tremblay, A., and Varfalvy, L.: Gas transfer velocities of  $\text{CO}_2$  and  $\text{CH}_4$  in a tropical reservoir and its river downstream, *J. Mar. Syst.*, 66, 161–172, <https://doi.org/10.1016/j.jmarsys.2006.03.019>, 2007.
- Ho, D. T., Engel, V. C., Ferrón, S., Hickman, B., Choi, J., and Harvey, J. W.: On factors influencing air-water gas exchange in emergent wetlands, *J. Geophys. Res.-Biogeo.*, 123, 178–192, <https://doi.org/10.1002/2017JG004299>, 2018.
- Hope, D., Billett, M., and Cresser, M.: A review of the export of carbon in river water: fluxes and processes, *Environ. Pollut.*, 84, 301–324, [https://doi.org/10.1016/0269-7491\(94\)90142-2](https://doi.org/10.1016/0269-7491(94)90142-2), 1994.
- Hope, D., Palmer, S. M., Billett, M. F., and Dawson, J. J. H. P.: Variations in dissolved  $\text{CO}_2$  and  $\text{CH}_4$  in a first-order stream and catchment: an investigation of soil–stream linkages, *J. Hydrol. Process.*, 18, 3255–3275, <https://doi.org/10.1002/hyp.5657>, 2004.
- Hotchkiss, E., Hall Jr, R., Sponseller, R., Butman, D., Klamin-der, J., Laudon, H., Rosvall, M., and Karlsson, J. J. N. G.: Sources of and processes controlling  $\text{CO}_2$  emissions change with the size of streams and rivers, *Nat. Geosci.*, 8, 696–699, <https://doi.org/10.1038/ngeo2507>, 2015.
- Jeffrey, L. C., Santos, I. R., Tait, D. R., Makings, U., and Maher, D. T.: Seasonal drivers of carbon dioxide dynamics in a hydrologically modified subtropical tidal river and estuary (Caboolture River, Australia), *J. Geophys. Res.-Biogeo.*, 123, 1827–1849, <https://doi.org/10.1029/2017jg004023>, 2018.
- Johnson, M. S., Weiler, M., Couto, E. G., Riha, S. J., and Lehmann, J.: Storm pulses of dissolved  $\text{CO}_2$  in a forested headwater Amazonian stream explored using hydrograph separation, *Water Resour. Res.*, 43, W11201, <https://doi.org/10.1029/2007WR006359>, 2007.
- Johnson, M. S., Lehmann, J., Riha, S. J., Krusche, A. V., Richey, J. E., Ometto, J. P. H., and Couto, E. G.:  $\text{CO}_2$  efflux from Amazonian headwater streams represents a significant fate for deep soil respiration, *Geophys. Res. Lett.*, 35, L17401, <https://doi.org/10.1029/2008GL034619>, 2008.
- Kalbitz, K. and Kaiser, K.: Contribution of dissolved organic matter to carbon storage in forest mineral soils, *J. Plant Nutr. Soil Sci.*, 171, 52–60, <https://doi.org/10.1002/jpln.200700043>, 2008.
- Lambert, T., Bouillon, S., Darchambeau, F., Morana, C., Roland, F. A. E., Descy, J.-P., and Borges, A. V.: Effects of human land use on the terrestrial and aquatic sources of fluvial organic matter in a temperate river basin (The Meuse River, Belgium), *Biogeochemistry*, 136, 191–211, <https://doi.org/10.1007/s10533-017-0387-9>, 2017.
- Lauerwald, R., Laruelle, G. G., Hartmann, J., Ciais, P., and Regnier, P. A.: Spatial patterns in  $\text{CO}_2$  evasion from the global river network, *Global Biogeochem. Cy.*, 29, 534–554, <https://doi.org/10.1002/2014GB004941>, 2015.
- Le Coz, J., Pierrefeu, G., and Paquier, A.: Evaluation of river discharges monitored by a fixed side-looking Doppler profiler, *Water Resour. Res.*, 44, W00D09, <https://doi.org/10.1029/2008WR006967>, 2008.
- Le, T. P. Q., Marchand, C., Ho, C. T., Da Le, N., Duong, T. T., Lu, X., Doan, P. K., Nguyen, T. K., Nguyen, T. M. H., and Vu, D. A.:  $\text{CO}_2$  partial pressure and  $\text{CO}_2$  emission along the lower Red River (Vietnam), *Biogeosciences*, 15, 4799–4814, <https://doi.org/10.5194/bg-15-4799-2018>, 2018.
- Li, S., Lu, X. X., and Bush, R. T.:  $\text{CO}_2$  partial pressure and  $\text{CO}_2$  emission in the Lower Mekong River, *J. Hydrol.*, 504, 40–56, <https://doi.org/10.1016/j.jhydrol.2013.09.024>, 2013.
- Li, S., Ni, M., Mao, R., and Bush, R. T.: Riverine  $\text{CO}_2$  supersaturation and outgassing in a subtropical monsoonal mountainous area (Three Gorges Reservoir Region) of China, *J. Hydrol.*, 558, 460–469, <https://doi.org/10.1016/j.jhydrol.2018.01.057>, 2018.
- Li, X., Xu, J., Shi, Z., and Li, R.: Response of Bacterial Metabolic Activity to the River Discharge in the Pearl River Estuary: Implication for  $\text{CO}_2$  Degassing Fluxes, *Front. Microbiol.*, 10, 1026, <https://doi.org/10.3389/fmicb.2019.01026>, 2019.
- Liang, B., Hu, J. T., Li, S. Y., Ye, Y. X., Liu, D. H., and Huang, J.: Carbon system simulation in the Pearl River Estuary, China: Mass fluxes and transformations, *J. Geophys. Res.-Biogeo.*, 125, e2019JG005012, <https://doi.org/10.1029/2019jg005012>, 2020.
- Luo, J., Li, S., Ni, M., and Zhang, J.: Large spatiotemporal shifts of  $\text{CO}_2$  partial pressure and  $\text{CO}_2$  degassing in a monsoonal headwater stream, *J. Hydrol.*, 579, 124135, <https://doi.org/10.1016/j.jhydrol.2019.124135>, 2019.

- Marx, A., Dusek, J., Jankovec, J., Sanda, M., Vogel, T., van Geldern, R., Hartmann, J., and Barth, J. A. C.: A review of  $\text{CO}_2$  and associated carbon dynamics in headwater streams: A global perspective, *Rev. Geophys.*, 55, 560–585, <https://doi.org/10.1002/2016rg000547>, 2017.
- Millero, F. J., Graham, T. B., Huang, F., Bustos-Serrano, H., and Pierrot, D.: Dissociation constants of carbonic acid in seawater as a function of salinity and temperature, *Mar. Chem.*, 100, 80–94, <https://doi.org/10.1016/j.marchem.2005.12.001>, 2006.
- Moramarco, T., Saltalippi, C., and Singh, V. P.: Estimation of Mean Velocity in Natural Channels Based on Chiu's Velocity Distribution Equation, *J. Hydrol. Eng.*, 9, 42–50, [https://doi.org/10.1061/\(ASCE\)1084-0699\(2004\)9:1\(42\)](https://doi.org/10.1061/(ASCE)1084-0699(2004)9:1(42)), 2004.
- Müller-Dum, D., Warneke, T., Rixen, T., Müller, M., Baum, A., Christodoulou, A., Oakes, J., Eyre, B. D., and Notholt, J.: Impact of peatlands on carbon dioxide ( $\text{CO}_2$ ) emissions from the Rajang River and Estuary, Malaysia, *Biogeosciences*, 16, 17–32, <https://doi.org/10.5194/bg-16-17-2019>, 2019.
- Ni, M., Li, S., Luo, J., and Lu, X.:  $\text{CO}_2$  partial pressure and  $\text{CO}_2$  degassing in the Daning River of the upper Yangtze River, China, *J. Hydrol.*, 569, 483–494, <https://doi.org/10.1016/j.jhydrol.2018.12.017>, 2019.
- Ran, L., Lu, X. X., Yang, H., Li, L., Yu, R., Sun, H., and Han, J.:  $\text{CO}_2$  outgassing from the Yellow River network and its implications for riverine carbon cycle, *J. Geophys. Res.-Biogeo.*, 120, 1334–1347, <https://doi.org/10.1002/2015jg002982>, 2015.
- Ran, L., Li, L., Tian, M., Yang, X., Yu, R., Zhao, J., Wang, L., and Lu, X.: Riverine  $\text{CO}_2$  emissions in the Wuding River catchment on the Loess Plateau: Environmental controls and dam impoundment impact, *J. Geophys. Res.-Biogeo.*, 122, 1439–1455, <https://doi.org/10.1002/2016JG003713>, 2017a.
- Ran, L., Lu, X. X., and Liu, S.: Dynamics of riverine  $\text{CO}_2$  in the Yangtze River fluvial network and their implications for carbon evasion, *Biogeosciences*, 14, 2183–2198, <https://doi.org/10.5194/bg-14-2183-2017>, 2017b.
- Ran, L., Lu, X., Fang, N., and Yang, X.: Effective soil erosion control represents a significant net carbon sequestration, *Sci. Rep.*, 8, 12018, <https://doi.org/10.1038/s41598-018-30497-4>, 2018.
- Ran, Y., Li, X., Lu, L., and Li, Z.: Large-scale land cover mapping with the integration of multi-source information based on the Dempster–Shafer theory, *Int. J. Geogr. Inf. Sci.*, 26, 169–191, [doi:10.1080/13658816.2011.577745](https://doi.org/10.1080/13658816.2011.577745), 2012.
- Rasera, M. d. F. F., Krusche, A. V., Richey, J. E., Ballester, M. V., and Victoria, R. L.: Spatial and temporal variability of  $p\text{CO}_2$  and  $\text{CO}_2$  efflux in seven Amazonian Rivers, *Biogeochemistry*, 116, 241–259, <https://doi.org/10.1007/s10533-013-9854-0>, 2013.
- Raymond, P. A., Zappa, C. J., Butman, D., Bott, T. L., Potter, J., Mulholland, P., Laursen, A. E., McDowell, W. H., and Newbold, D.: Scaling the gas transfer velocity and hydraulic geometry in streams and small rivers, *Limnol. Oceanogr.-Fluid. Environ.*, 2, 41–53, <https://doi.org/10.1215/21573689-1597669>, 2012.
- Raymond, P. A., Hartmann, J., Lauerwald, R., Sobek, S., McDonald, C., Hoover, M., Butman, D., Striegl, R., Mayorga, E., and Humborg, C.: Global carbon dioxide emissions from inland waters, *Nature*, 503, 355–359, <https://doi.org/10.1038/nature12760>, 2013.
- Reiman, J. H. and Xu, Y. J.: Diel Variability of  $p\text{CO}_2$  and  $\text{CO}_2$  Outgassing from the Lower Mississippi River: Implications for Riverine  $\text{CO}_2$  Outgassing Estimation, *Water*, 11, 43, <https://doi.org/10.3390/w11010043>, 2019a.
- Reiman, J. H. and Xu, Y. J.: Dissolved carbon export and  $\text{CO}_2$  outgassing from the lower Mississippi River – Implications of future river carbon fluxes, *J. Hydrol.*, 578, 124093, <https://doi.org/10.1016/j.jhydrol.2019.124093>, 2019b.
- Rocher-Ros, G., Sponseller, R. A., Lidberg, W., Mörth, C. M., and Giesler, R.: Landscape process domains drive patterns of  $\text{CO}_2$  evasion from river networks, *Limnol. Oceanogr. Lett.*, 4, 87–95, <https://doi.org/10.1002/lol2.10108>, 2019.
- Sawakuchi, H. O., Neu, V., Ward, N. D., Barros, M. d. L. C., Valerio, A. M., Gagne-Maynard, W., Cunha, A. C., Less, D. F. S., Diniz, J. E. M., Brito, D. C., Krusche, A. V., and Richey, J. E.: Carbon dioxide emissions along the lower Amazon River, *Front. Mar. Sci.*, 4, 76, <https://doi.org/10.3389/fmars.2017.00076>, 2017.
- Stets, E. G., Butman, D., McDonald, C. P., Stackpoole, S. M., DeGrandpre, M. D., and Striegl, R. G.: Carbonate buffering and metabolic controls on carbon dioxide in rivers, *Global Biogeochem. Cy.*, 31, 663–677, <https://doi.org/10.1002/2016gb005578>, 2017.
- Tao, Z., Gao, Q., Wang, Z., Zhang, S., Xie, C., Lin, P., Ruan, X., Li, S., and Mao, H.: Estimation of carbon sinks in chemical weathering in a humid subtropical mountainous basin, *Chin. Sci. Bull.*, 56, 3774–3782, <https://doi.org/10.1007/s11434-010-4318-6>, 2011.
- Teodoru, C. R., Nyoni, F. C., Borges, A. V., Darchambeau, F., Nyambe, I., and Bouillon, S.: Dynamics of greenhouse gases ( $\text{CO}_2$ ,  $\text{CH}_4$ ,  $\text{N}_2\text{O}$ ) along the Zambezi River and major tributaries, and their importance in the riverine carbon budget, *Biogeosciences*, 12, 2431–2453, <https://doi.org/10.5194/bg-12-2431-2015>, 2015.
- Tian, M., Yang, X., Ran, L., Su, Y., Li, L., Yu, R., Hu, H., and Lu, X. X.: Impact of land cover types on riverine  $\text{CO}_2$  outgassing in the Yellow River source region, *Water*, 11, 2243, <https://doi.org/10.3390/w11112243>, 2019.
- Wanninkhof, R.: Relationship between wind speed and gas exchange over the ocean, *J. Geophys. Res.-Ocean.*, 97, 7373–7382, <https://doi.org/10.1029/92JC00188>, 1992.
- Weiss, R. F.: Carbon dioxide in water and seawater: the solubility of a non-ideal gas, *Mar. Chem.*, 2, 203–215, [https://doi.org/10.1016/0304-4203\(74\)90015-2](https://doi.org/10.1016/0304-4203(74)90015-2), 1974.
- Xuan, Y., Cao, Y., Tang, C., and Li, M.: Changes in dissolved inorganic carbon in river water due to urbanization revealed by hydrochemistry and carbon isotope in the Pearl River Delta, China, *Environ. Sci. Pollut. Res.*, 27, 24542–24557, <https://doi.org/10.1007/s11356-020-08454-4>, 2020.
- Yao, G., Gao, Q., Wang, Z., Huang, X., He, T., Zhang, Y., Jiao, S., and Ding, J.: Dynamics of  $\text{CO}_2$  partial pressure and  $\text{CO}_2$  outgassing in the lower reaches of the Xijiang River, a subtropical monsoon river in China, *Sci. Total Environ.*, 376, 255–266, <https://doi.org/10.1016/j.scitotenv.2007.01.080>, 2007.
- Zhang, L., Qin, X., Liu, P., Huang, Q., Lan, F., and Ji, H.: Estimation of carbon sink fluxes in the Pearl River basin (China) based on a water–rock–gas–organism interaction model, *Environ. Earth Sci.*, 74, 945–952, <https://doi.org/10.1007/s12665-014-3788-2>, 2015.
- Zhang, S., Lu, X. X., Higgitt, D. L., Chen, C.-T. A., Han, J., and Sun, H.: Recent changes of water discharge and sediment load in the Zhujiang (Pearl River) Basin, China, *Glob. Planet. Change*,

- 60, 365–380, <https://doi.org/10.1016/j.gloplacha.2007.04.003>, 2008.
- Zhang, T., Li, J., Pu, J., and Yuan, D.: Carbon dioxide exchanges and their controlling factors in Guijiang River, SW China, *J. Hydrol.*, 578, 124073, <https://doi.org/10.1016/j.jhydrol.2019.124073>, 2019.
- Zhang, W., Li, H., Xiao, Q., and Li, X.: Urban rivers are hotspots of riverine greenhouse gas ( $\text{N}_2\text{O}$ ,  $\text{CH}_4$ ,  $\text{CO}_2$ ) emissions in the mixed-landscape chaohu lake basin, *Water Res.*, 189, 116624, <https://doi.org/10.1016/j.watres.2020.116624>, 2021.